Compact real-time RF spectrum analyzer with 16 GHz instantaneous bandwidth based on photonic frequency-shifting loops

Hugues Guillet de Chatellus

Research Article Vol. 2, No. 6 / 15 Jun 2023 / Optics Continuum 1276
OPTICS CONTINUUM

Compact real-time RF spectrum analyzer with 16 GHz instantaneous bandwidth based on photonic frequency-shifting loops

HUGUES GUILLET DE CHATELLUS[1,2,*]

[1]Laboratoire Interdisciplinaire de Physique, UGA/CNRS, 38000 Grenoble, France
[2]Univ Rennes, CNRS, Institut FOTON - UMR 6082, 35000 Rennes, France
[*]hugues.guilletdechatellus@univ-rennes1.fr

Abstract: Spectral analysis of broadband RF signals in real time is of primary importance for numerous applications. So far, the instantaneous bandwidth of real-time spectrum analyzers based on conventional digital techniques is limited to a few GHz. This limitation is set by the clock jitter of the analog-to-digital converters, and by the processing capabilities in real time of digital electronics. On the contrary, analog architectures based on microwave photonics are not constrained by such limitations, and offer potentially a very high instantaneous bandwidth. However, they generally suffer from inherent limitations, such as large footprint and high complexity. Here, we propose a much simpler architecture of RF spectrum analyzer based on frequency-shifting loops. It utilizes only compact commercial telecom components, a single CW laser, and slow electronic resources (10 MSa/s). The probability of intercept is 100%, the instantaneous bandwidth reaches 16 GHz, and the spectral and temporal resolutions are respectively equal to 160 MHz and 50 µs. Our system is expected to open new avenues in embedded applications of microwave photonics.

1. Introduction

Spectral characterization of fast radio-frequency (RF) waveforms in real time is a critical issue in numerous domains, ranging from telecommunications, remote sensing (radar, lidar), radio astronomy, spectroscopy, science applications, and electronic warfare. Conventional electronic instrumentation for spectral analysis of electrical signals comprises heterodyne sweep spectrum analyzers (SSA), and digital real-time spectrum analyzers (RTSA) [1]. In SSAs, the RF signal under test (SUT) is mixed with a local oscillator, whose frequency is scanned over the SUT bandwidth. The spectral resolution and the dynamic range of SSAs can be very high, but at the expense of long acquisition times. Additionally, SSAs are restricted to signals with stationary spectrum, and are not adapted to sparse signals or to signals whose spectrum changes over time. On the contrary, RTSAs lift this limitation, since they digitize in real time the input signal by means of a fast analog-to-digital converter, and compute on the fly the instantaneous spectrum of the SUT [2,3]. However, both steps set stringent limitations to the maximum instantaneous bandwidth of the SUT. First, the inherent jitter of analog-to-digital converters limits the fidelity of the digitization, by reducing the effective number of bits of the sampled signal [4]. Second, processing several 10^9 samples per second in real time requires excessively large computing resources. In practice, despite spectacular improvements of digital techniques over the last 30 years, the real-time instantaneous bandwidth of commercial RTSAs is still limited to a few GHz. Yet spectral analysis of signal with multi GHz bandwidth is a crucial issue, since large bandwidth is associated with high resolution in ranging experiments, high data rates in telecommunications, and low probability of intercept in defense applications.

On the other hand, analog techniques are natural candidates to go beyond the limits of digital electronics: the SUT does not need to be sampled nor digitized, and the processing is achieved by

#485987 https://doi.org/10.1364/OPTCON.485987
Journal © 2023 Received 18 Jan 2023; revised 7 Apr 2023; accepted 26 Apr 2023; published 16 May 2023

OPTICS CONTINUUM

means of physical processes, including interference and detection itself. Additionally, transferring and processing RF signals into the optical domain enables to get rid of the bandwidth limitations of electronic and RF components, by taking advantage of the huge bandwidth of optical components.

A first class of analog techniques based on optics makes use of diffraction in a crystal doped with rare-earth ions at low temperature, where a grating with a ultrahigh dispersion has been induced [5,6]. The spectrum of the SUT is directly measured on a camera. These techniques have proven a very high level of performance: the instantaneous analysis bandwidth is beyond 40 GHz, the spur free dynamic range exceeds 60 dB, while the spectral and temporal resolutions are typically 100 MHz and 20 μs. However, these techniques are limited by the intrinsic complexity of the system, a poor SWaP-C (size, weight, power and cost), a large power consumption, and the need for cryo-cooling, which forbid till now onboard integration of the system.

A second class of analog techniques for spectral analysis relates to microwave photonics [7,8]. Various approaches demonstrated so far exploit the space-time duality - i.e. the correspondence between the diffraction of wavefronts in free space, and the propagation of waveforms through dispersive media [9]. Among them, so-called dispersive Fourier transform is strikingly simple, and especially adapted to signals with extremely large bandwidth [10,11]. However, it is restricted to time-limited or truncated input signals, and its spectral resolution is poor, well above the GHz range. On the other hand, techniques using time lenses show improved frequency resolution, but are limited by the experimental challenge of implementing time lenses with the desired parameters [12].

More recently, techniques based on periodic sampling combined to dispersion have emerged, and constitute interesting alternatives to conventional approaches based on space-time duality [8]. Two different systems have been reported. In [13], authors make use of a train of mode-locked pulses to sample the SUT. In the Fourier domain, the spectrum consists of replicas of the SUT spectrum, spaced by the sampling frequency. After propagation in a dispersive medium with a specific group delay dispersion, the intensity reproduces periodically the power spectrum of the SUT. A related approach has been investigated in [14]: replicas of the input spectrum are created by recirculation of the input signal in a frequency-shifting loop (FSL). Simultaneously, a quadratic spectral phase is imprinted on the frequency-shifted replicas by the recirculation process itself, mimicking the dispersive propagation of [13]. In these approaches, a similar role is played by the sampling frequency in [13] (i.e. the repetition rate of the pulse train), and by the frequency shift per round-trip in [14]. If one denotes this value by f_s, it can be shown that in both cases, the spectral bandwidth of the SUT should not exceed f_s. Moreover, the SUT spectrum is mapped within a single period of the output signal (period: $1/f_s$). Therefore, extracting the spectrum requires the sampling rate of the output signal to be larger than the bandwidth of the SUT. In other words, although the computation of the SUT spectrum is performed in an analog fashion, its recording requires comparable resources to what would be required for conventional digital RTSA. This constraint is a critical hurdle to the development of techniques based on periodic sampling.

In this letter, we propose a novel technique of analog spectrum analysis in real time based on FSLs [15]. We show that the addition of a second FSL enables to lift the stringent requirement of periodic sampling-based techniques in terms of detection bandwidth. More precisely, the real-time instantaneous bandwidth of our system is 16 GHz, while the bandwidth of the processing chain does not exceed 5 MHz. The spectral and temporal resolutions of the technique are respectively 160 MHz and 50 μs, and the probability of interception is 100%. Our systems currently offers a dynamic range of 20 dB, limited by the saturation of the optical amplifier, a value that could theoretically be enhanced up to 47 dB. Most importantly, the hardware is much more simple and compact than previous photonic-based techniques developed so far: it involves a CW single frequency laser, commercial fiber components at the telecom wavelength and slow electronics, which potentially makes the architecture easily deployable on the field.

OPTICS CONTINUUM

2. System description

2.1. Bidirectional frequency-shifting loop

The architecture proposed here combines two acousto-optic frequency-shifting loops (FSLs) [16,17]. Recall that a (single) FSL consists of a fiber loop that contains the following elements: a pair of couplers to inject and extract the light from the loop, an acousto-optic frequency shifter, and an amplifier. The role of the latter is to compensate for the transmission losses in the loop. The FSL also contains a tunable bandpass filter, so as to limit the amplified spontaneous emission (ASE) that circulates in the loop, and to control the spectral bandwidth at the FSL output, i.e. the number of round-trips of the light in the loop [17]. A FSL is essentially described by two parameters: its travel time τ_c, set by the total length of the loop, and the frequency shift per round-trip f_s (i.e. the frequency applied to the acousto-optic modulator). In microwave photonics-based applications, the loop is seeded by a single frequency laser modulated by the RF SUT by means of a Mach-Zehnder modulator biased at null point. In the case where the product $f_s\tau_c$ is an integer, it has been shown that, provided the SUT bandwidth is smaller than $1/\tau_c$, the signal at the FSL output reproduces the spectrum of the input SUT with a repetition rate of f_s (typ. 80 MHz) [14,18]. In practice, the SUT bandwidth should not exceed a few tens of MHz ($1/\tau_c$ is in the 10s MHz range). Additionally, as said in the introduction, the output signal should be sampled at several GSa/s, which restricts the practical interest of the single FSL architecture for spectrum analysis.

To lift this double limitation, we combine here two FSLs into a single bidirectional FSL (denoted "Bi-FSL") seeded in both ways by a CW laser modulated by the SUT [19–21] (Fig. 1). The amplifier and the filter are both bidirectional. A non-reciprocal section, made of circulators, delay lines and frequency shifters, enables to control the frequency shifts and the travel times of both ways independently (see inset in Fig. 1). Fractions of the signals circulating in the FSLs are extracted by means of two couplers, and are recombined on a balanced photodetector.

2.2. Theoretical analysis

A brief mathematical analysis of the system demonstrating its capability for spectrum analysis is given in the following. The (complex) electric field injected in the loop is equal to: $E_0 s(t) e^{i2\pi f_0 t}$, where E_0 and f_0 are respectively the amplitude and the frequency of the CW seed laser, $s(t)$ is the input RF signal applied to the amplitude modulator. The auto-correlation function of s is defined by: $R_{ss}(\tau) = \langle s(t)s(t-\tau)\rangle$, and is related to the power spectrum by $FT[R_{ss}](f) = S(f)$, where FT denotes the Fourier transform.

We designate τ_1 and τ_2 as the travel times of the light in the FSLs. Similarly, f_1 and f_2 are the frequency shifts per round-trip. We also define: $\Delta\tau = \tau_2 - \tau_1$ and $\Delta f = f_1 - f_2$. We suppose that the tunable optical bandpass filter in the Bi-FSL has a flat-top response, and that f_0 corresponds to the low frequency edge of filter, the frequency shifts f_1 and f_2 being positive. We define N as the ratio between the filter's bandwidth and the frequency shift $f_1 \approx f_2$. N interprets also as the number of round-trips of the light in the loop. Then, the complex electric fields at the output of the loop in paths #1 and #2 are respectively equal to [21]:

$$E_{1,2}(t) = E_0 e^{i2\pi f_0 t} \sum_{n=0}^{N} \eta^n s(t - n\tau_{1,2}) e^{i2\pi n f_{1,2} t} e^{-i\pi f_{1,2}\tau_{1,2} n^2}. \quad (1)$$

A linear phase term has been omitted here, since it only translates into a global time shift of the output signal. The parameter η can be seen as the net gain per round-trip in the FSL. It is equal to the product of the amplifier's gain by the transmission coefficient of the loop (single pass). For simplicity, we assume that the value of η is set equal to unity.

OPTICS CONTINUUM

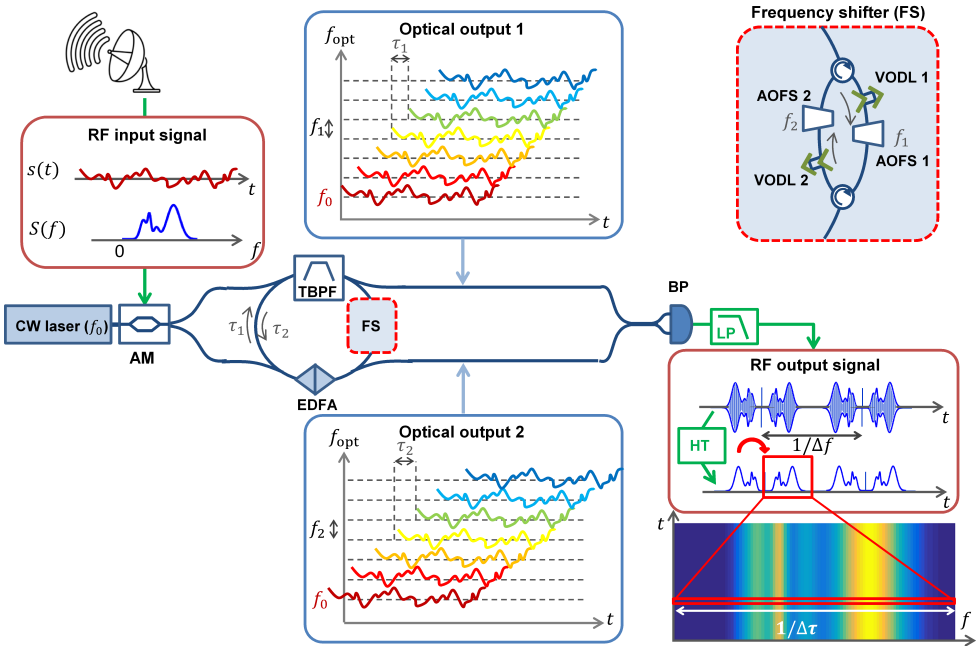

Fig. 1. Experimental set-up. The RF input signal under test (SUT) is transferred into the optical domain by amplitude modulation of a single frequency CW laser (frequency: f_0). The optical signal is split, and seeds from both ways a bi-directional FSL, containing a tunable bandpass filter (TBPF), an amplifier (EDFA), and a non-reciprocal frequency shifter (inset in the top right). The latter comprises pairs of circulators, of acousto-optic frequency shifters (AOFS) and of variable optical delay lines (VODL), which enable to control the frequency shifts (f_1 and f_2) and the travel times (τ_1 and τ_2) in the loops. The Bi-FSL generates replicas on the input signal, shifted both along the time, and the frequency domain. The optical output signals are recombined on a balanced photodetector (BP). After low-pass filtering (LP), the signal is digitized and numerically processed. The modulus of the Hilbert transform (HT) maps in time the double-sided power spectrum of the input signal. The single-sided spectrum is then extracted, and displayed as a spectrogram.

$E_1(t)$ and $E_2(t)$ are recombined on a balanced photodetector. The photocurrent is proportional to the light intensity and writes:

$$I(t) = w(t) * [E_1(t)E_2^*(t)] + C.C. \tag{2}$$

where $w(t)$ is the time impulse response of the detection chain (detector, LP filter), $*$ stands for the convolution product, and $C.C.$ denotes the complex conjugate. Defining $I_0 = E_0E_0^*$ leads to:

$$E_1(t)E_2^*(t) = I_0 \sum_{n,m} s(t - n\tau_1)s(t - m\tau_2)e^{i2\pi(nf_1 - mf_2)t}e^{-i\pi(f_1\tau_1 n^2 - f_2\tau_2 m^2)}. \tag{3}$$

Calculations derived in [21] show that, after low-pass filtering (cut-off frequency: $N\Delta f$), for most signals, only terms where $n = m$ contribute significantly to the previous sum. Then:

$$I(t) \propto \sum_n \langle s(t)s(t - n\Delta\tau)\rangle e^{i2\pi n\Delta ft}e^{-i\pi(f_1\tau_1 - f_2\tau_2)n^2} + C.C. \tag{4}$$

where $\langle\rangle$ denotes the temporal average over a duration set by the impulse response $w(t)$. Assuming that $f_1\tau_1 = f_2\tau_2$,

$$I(t) \propto \sum_n R_{ss}(n\Delta\tau)e^{i2\pi n\Delta ft} + C.C. \tag{5}$$

OPTICS CONTINUUM

Finally, owing to the Poisson summation formula:

$$I(t) \propto \sum_n S\left(\frac{\Delta f}{\Delta \tau} t - \frac{n}{\Delta \tau}\right) + C.C. \tag{6}$$

This expression highlights a frequency-to-time mapping phenomenon: the output signal $I(t)$ reproduces periodically along time (period: $1/\Delta f$) the real part of the power spectrum of the input signal $s(t)$. As expected, the period of the output signal, i.e. the temporal resolution of the technique, is $1/\Delta f$. The coefficient of the frequency-to-time mapping (i.e. the ratio between the time scale of the output signal and the frequency scale of the input one) is $\Delta\tau/\Delta f$. If the bandwidth of the input signal exceeds $1/(2\Delta\tau)$, then the output traces begin to overlap (the factor $1/2$ comes from the fact that the real part of the power spectrum contains negative and positive frequency components). Therefore the spectral bandwidth of the technique is equal to $1/(2\Delta\tau)$. The frequency resolution δf is given by the inverse of the product between the bandwidth of the output signal and the frequency-to-time mapping coefficient. In other words, $\delta f = \Delta f/(N\Delta f \times \Delta\tau) = 1/(N\Delta\tau)$. Interestingly the ratio between the bandwidth and the frequency resolution, or time-bandwidth product, is simply equal to $N/2$.

2.3. Detection and processing

The output signal $I(t)$ is detected by means of a balanced photodetector followed by a low-pass filter, whose cut-off frequency is just above $N\Delta f$. The output signal is digitized and processed by means of an acquisition board and a computer. The digital signal is divided into individual

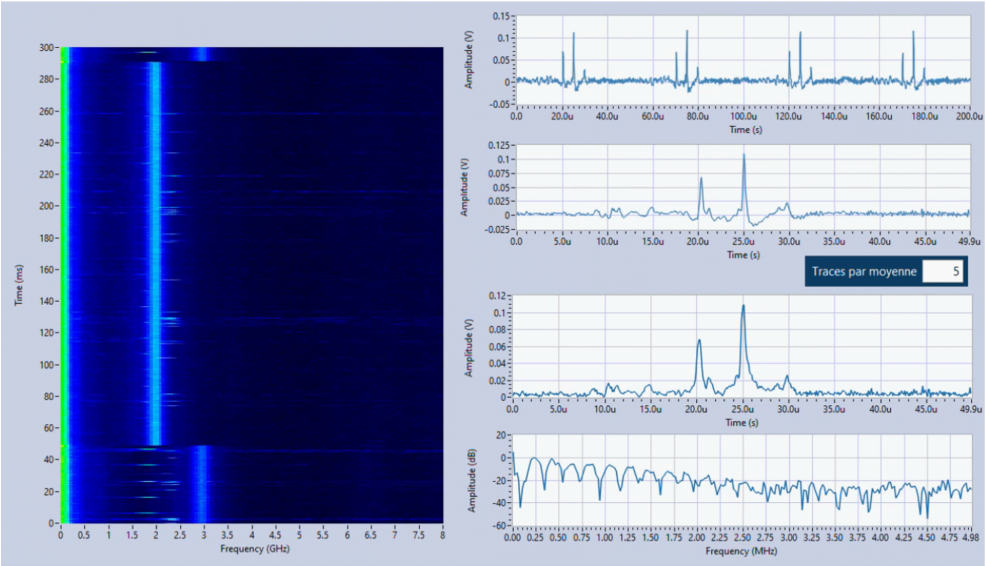

Fig. 2. Screenshot of the system interface. The top plot on the right panel is the raw signal acquired by the balanced photodetector. In the case of a monochromatic input signal, it consists of three pulses. The central pulse corresponds to the null frequency, while the side ones correspond to the negative and positive frequency components of the SUT (see text). The second and third plots are respectively a single period and an average of the modulus of the Hilbert transform of the output signal over a single period (50 µs). The fourth plot is the power spectrum of the averaged Hilbert transform. The left panel displays the spectrogram, i.e. the power spectrum (horizontal scale) as a function of time (vertical scale). For clarity, the frequency scale has been reduced to the range 0-8 GHz.

OPTICS CONTINUUM

periods of duration $1/\Delta f$. Since the output signal maps the real part of the power spectrum of the SUT, a Hilbert transform is applied on the fly to the individual periods. The modulus of the Hilbert transform is proportional to the power spectrum of the SUT. For a monochromatic input signal, an individual period (after Hilbert transform) consists of a doublet, corresponding to the negative and positive frequency components of the SUT. The spacing of the pulse doublet is proportional to twice the frequency of the input SUT. As said, the AM is a Mach-Zehnder electro-optic modulator biased at null point. However, a slight detuning of the bias leads to the appearance of an additional peak at the center of the doublet. This central peak stands for the null frequency. The individual traces are then numerically folded with respect to the central peak, so that the two pulses corresponding to the positive and negative frequencies overlap. The folded traces are then displayed over time in a spectrogram plot, where the horizontal axis is the frequency scale, and the vertical one is the time. A screenshot of the system interface summarizing the signal processing is displayed in Fig. 2.

3. Experimental results

A Bi-FSL has been implemented with polarization-maintaining fiber components. All components are commercially available. The seed laser is a narrow-linewidth laser (< 1 kHz linewidth) delivering 10 dBm at 1550 nm. The amplitude modulator is a conventional Lithium Niobate Mach-Zehnder interferometer (20 GHz bandwidth, 30 dB extinction ratio, V_π = 5.5 V). The amplifier is a bidirectional EDFA. The pump diode current is set to achieve transparency, so that the gain per roundtrip exactly compensates for the losses. The bidirectional bandpass filter is tunable both in central wavelength and in spectral bandwidth (minimum FWHM spectral bandwidth: 0.35 nm at 1550 nm, filter edge rolling-off slope: 100 dB/nm). The total length of the fiber bidirectional loop is slightly less than 30 meters. The frequencies of the AOFS are respectively set to 80.020 MHz and 80.000 MHz (Δf = 20 kHz). When no input RF signal is applied to the seed laser, the Bi-FSL generates an (optical) dual-comb with respective spacings f_1 and f_2, and total bandwidths Nf_1 and Nf_2. The heterodyne signal restricted to the first Ny-Quist zone consists of an RF comb, with a spacing of Δf and a bandwidth of $N\Delta f$. Measuring the RF comb provides an experimental measurement of N [19]. Experimentally, the TBPF is set, so that $N \simeq 200$. Then the values of τ_1 and τ_2 are set by means of the VODLs in the non-reciprocal frequency shifter so as to satisfy $f_1\tau_1 = f_2\tau_2 = 10.00$. (This value is measured by determining the temporal Talbot conditions of both loops, see [17]). Consequently, $\Delta\tau$ = 31.2 ps, and the corresponding frequency bandwidth is 16 GHz. The theoretical temporal and frequency resolutions of the system are respectively equal to $1/\Delta f$ = 50 µs, and to δf = 160 MHz. In the detection chain, the bandwidth of the balanced detector is 75 MHz, the cut-off frequency of the low-pass filter is 4.5 MHz ($\leq N\Delta f$), and the sampling rate of the acquisition board is 10 MSa/s.

3.1. System performance

In a first set of experiments, we characterize the performance of the system. For this aim, an RF single tone delivered by a synthesizer (0-13 GHz) is applied to the amplitude modulator. The AM bias is slightly detuned from the null point. As expected, the Hilbert transform modulus of the output trace contains three peaks per period: a central peak corresponding to the null frequency, and two side peaks, whose delay with respect to the central one is proportional to the signal frequency (Fig. 3). Then, to characterize the frequency resolution and the linearity of the technique, the frequency of the synthesizer is set to 1.6 GHz (RF power : −10 dBm). A single trace is provided in Fig. 4(a). The spectral resolution is set by the width of the peaks (inset Fig. 4(a)). In our example, the full width at half maximum is close to 300 MHz, to be compared to the theoretical resolution of 160 MHz. The influence of the input RF power is illustrated in Fig. 4(b). At low RF powers (below −10 dBm), the amplitude of the output signal Hilbert transform increases linearly with the input power. When the latter is increased beyond −10 dBm,

OPTICS CONTINUUM

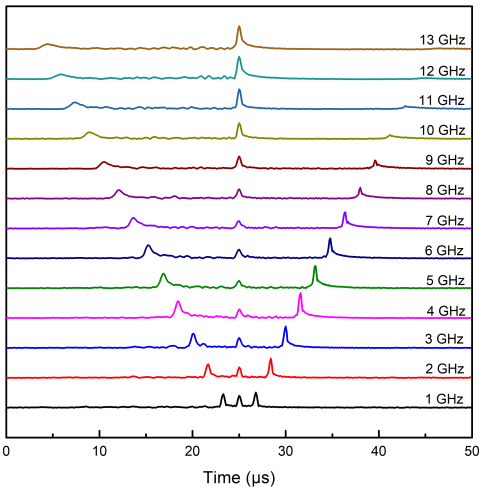

Fig. 3. Modulus of the Hilbert transform of a single output trace (50 µs) when the system is seeded by a single tone signal, as a function of the input frequency. Each trace is averaged 10 times.

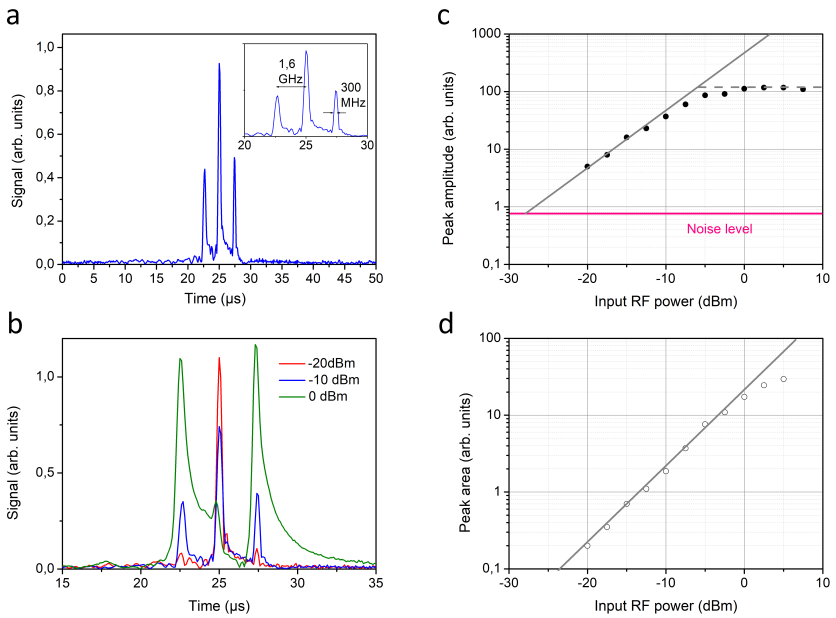

Fig. 4. a: Modulus of the Hilbert transform of a single output trace (50 µs) when the system is seeded by a single tone signal (frequency: 1.6 GHz, power: −10 dBm.) b: output traces for different values of the input signal power. c (resp. d): signal amplitude (resp. area of the peak) with respect to the input RF power. The straight lines (slope: 1) corresponds to the behaviors expected in the absence of saturation of the optical amplifier.

the output signal keeps increasing, but the satellite peaks simultaneously broaden. This effect is attributed to the saturation of the optical amplifier. Indeed, the optical power at the FSL input increases with the RF power applied to the AM, resulting in the saturation of the optical amplifier. Since the gain decreases, the signal power drops over the successive round-trips in the Bi-FSL

OPTICS CONTINUUM

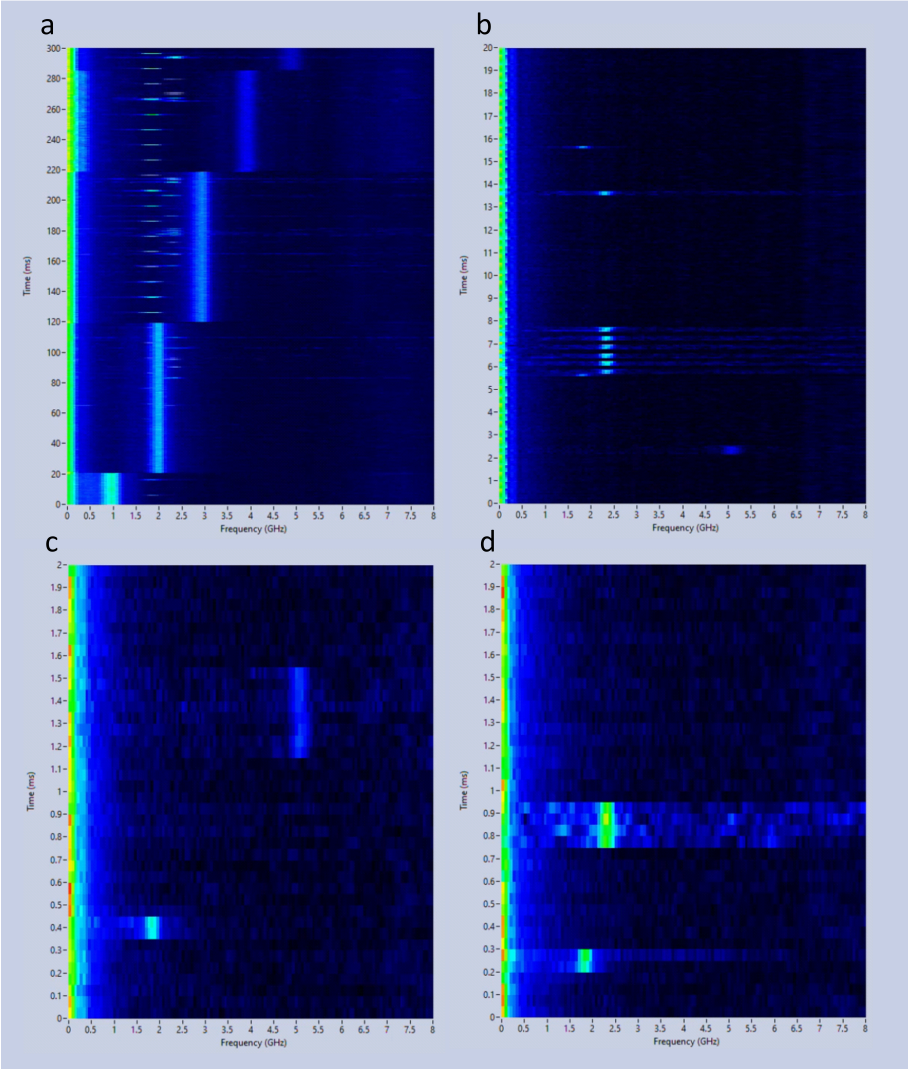

Fig. 5. Examples of spectrograms of the lab's ambient RF background for various integration times (a: 300 ms, b: 20 ms, and c, d: 2 ms). Different signals are detected, including wi-fi (2.4 GHz and 5.5 GHz) and mobile phones (1800 MHz) - see text. For clarity, the frequency scale has been reduced to the range 0-8 GHz.

[22]. Then, less replicas of the input signal are involved in the build-up of the output signal, resulting in a broadening of the satellited peaks, and in a decrease of the spectral resolution.

To quantify this effect, we plot in Fig. 4(c) the variation of the peak amplitude with the power of the RF signal. In the low power region, the sensitivity is determined by the noise level of the system set by the the ASE circulating in the loop. The measured sensitivity is −27 dBm. Then a linear variation is observed for input powers up to −5 dBm, where the peak amplitude starts to saturate. Consequently, the dynamic range of the technique in the linear regime (without compression) is slightly above 20 dB. Still, it is possible to enhance the value of the dynamic range at the cost of degrading the frequency resolution. If one considers the area of the peak instead of its height, Fig. 4(d) shows that the peak area remains linear up to an RF input power of 0 dBm, enhancing the value of the dynamic range approximately up to 27 dB.

OPTICS CONTINUUM

3.2. Spectrum analysis

In a second set of experiments, the input RF SUT is collected by means of a broadband horn antenna (700 MHz-18 GHz), amplified up to the typical power range −25 to −5 dBm (i.e. where the output signal depends linearly on the power of the SUT), and applied to the AM. The input signal collected by the antenna (i.e. the ambient RF background) has several contributions: a wi-fi repeater (frequency bands: 2.4 GHz, 5.5 GHz) and cell-phones (1800 MHz). Additionally, a synthesizer (0-20 GHz) connected to a broadband emitting antenna is used as an additional source of RF signals (Visualization 1). Figure 5(a) shows an example of the spectrogram acquired in real time, over a duration of 300 ms. Several frequency components are detectable: wi-fi signals at 2.4 GHz, phone signals at 1800 MHz, and the signal transmitted by the synthesizer, whose frequency was changed manually by steps of 1 GHz from 1 to 5 GHz. In Fig. 5(b), a 20 ms-long spectrogram is displayed, and clearly evidences the fine temporal structure of a wi-fi burst signal. Figure 5(c) highlights the temporal resolution of the system. The vertical scale is reduced to 2 ms. Two signals are visible : a cell-phone burst at 1800 MHz, and a wi-fi burst at 5.5 GHz. Both signals are detected with a temporal resolution of 50 µs. Figure 5(d) shows the influence of high-power input RF signals. The trace in the spectrogram induced by a high-power wi-fi burst (2.4 GHz) is broadened along the horizontal scale, while additional noise is generated over the duration of the burst. These features are attributed to saturation effects in the optical amplifier in the Bi-FSL.

4. Conclusion

We have reported a novel photonic architecture based on a Bi-FSL, enabling real-time spectral analysis of broadband RF signals. The instantaneous analysis bandwidth is 16 GHz, the frequency resolution is 160 MHz, and the time resolution is 50 μs. The unsaturated dynamic range is close to 20 dB. Moreover, the (analog) processing of the input SUT is gap-free, which sets the probability of interception to 100 %. Most importantly, our system is strikingly simple: it combines a single CW laser with standard and commercially available polarization-maintaining components at the telecom wavelength. No fast electronics is required, but a simple digitizer at 10 MSa/s, which easily allows on the fly signal processing. Therefore the compactness and simplicity of the architecture offer promising prospects for embedded applications.

The proposed architecture shows also a large degree of flexibility in terms of instantaneous bandwidth, spectral, as well as temporal resolution, and can be optimized depending on the targeted application. The instantaneous bandwidth is set by the optical bandwidth supported by the Bi-FSL, i.e. by the spectral bandwidth of the optical TBPF. The latter can be expanded, but due to the ASE emitted by the optical amplifier, it is challenging in practice to raise the number of round-trips in the FSL beyond a few hundreds [22]. Increasing the spectral bandwidth would imply larger frequency shifts per round-trip, a feature that could be done by using faster AOFS, or electro-optic frequency shifters. However, the ASE power generally grows with the frequency shift per round-trip [22], which sets a limitation to the instantaneous bandwidth of the technique. Regarding the frequency resolution, recall that the ratio between the spectral bandwidth and the resolution is equal to $N/2$, the number of round-trips in the FSL. $N/2$ interprets as the finesse of the spectrum analyzer, and is experimentally limited to a few hundreds. The temporal resolution of the technique is directly set by the acquisition rate Δf. In the present experiments, it is equal to 20 kHz. Similarly to dual-comb systems, the maximum acquisition rate would be $f_2/(2N)$ [23]. Assuming $N = 200$ leads to a maximum acquisition rate of 200 kHz, that is to say a temporal resolution of 5 μs. Such acquisition rate could be reached by using a faster acquisition chain (100 MSa/s) and optimizing the signal processing to maintain real-time capability.

The limits of the technique in terms of sensitivity and dynamic range are essentially set by two physical effects: the intrinsic noise and the non-linearities of the system. The main contribution to the noise is the ASE emitted by the optical amplifier in the Bi-FSL [22,24], while

OPTICS CONTINUUM

the non-linearities include the saturation of the optical amplifier, and of the amplitude modulator. Quantifying the sensitivity and dynamic range requires to define s_0, the optical power at the FSL input, and a_0, the ASE power generated by the amplifier in a frequency band equal to f_1 ($\simeq f_2$). $a_0 = n_{sp}hf_0(G-1)f_1$, where n_{sp} is the spontaneous emission factor (n_{sp}>1), and G is the amplifier's gain [22,24]. Following [24], an approached expression of the best-case sensitivity is $S = \frac{V_\pi^2 a_0 B}{2\pi^2 Z_m s_0 f_1}$, where B and Z_m are respectively the detection bandwidth and the modulator's impedance. For typical experimental values ($s_0 = 1\mu$W, $f_1 = 80$ MHz, G =10, $a_0 = 0.1$ nW, B = 4.5 MHz, $V_\pi = 5.5$ V and $Z_m = 50\ \Omega$), $S = -37$ dBm [24]. The difference with the experimental value reported here (−27 dBm) is likely due to extra noise sources not taken into account so far (detection noise, quantization noise). The sensitivity limits the dynamic range of the system on the side of low input power. On the high input power side, we have shown that the dynamic range is currently constrained by the saturation of the optical amplifier. In the regime of linear response of the system, the measured dynamic range is 20 dB, a value that can be extended up to 27 dB in the saturated regime, but at the price of a degraded frequency resolution. Several approaches are possible to delay the saturation of the amplifier and remain in the linear regime, including optimizing the parameters of the doped fiber, or retroacting on the input optical power at the FSL input. Work is currently underway in this regard. Beyond saturation effects of the optical amplifier, the nonlinearity of the input amplitude modulator sets another ultimate limit to the dynamic range. More precisely, we define the compression dynamic range (CDR) as the range of input RF powers for which the peak amplitude of the output signal is above noise (SNR = 1), and for which the peak power is compressed by 1 dB as compared to a linear response. It can be shown that the theoretical expression is given by: CDR = $P_{1\text{dB}}/S$ [24]. With the previous values of the experimental parameters, one obtains CDR = 47 dB, a value that interprets as the upper limit of the system dynamic range.

Funding. Université Grenoble Alpes (IDEX- IRS 2020); Centre National de la Recherche Scientifique (Prematuration 2021).

Acknowledgments. We thank Adélie Wagner and Adeline Dekooninck (Arcale Company), for the digital interface of the system. We also thank Geneviève Pourroy (CNRS) and Agnès Savignier (Valoritech) for their help in setting up the project.

Disclosures. The authors declare no conflicts of interest.

Data availability. Data underlying the results presented in this paper may be obtained from the authors upon request.

References

1. A. Basu, "An Introduction to Microwave Measurements," (CRC, 2014).
2. Tektronix, Fundamentals of Real-Time Spectrum Analysis. https://www.tek.com/spectrum-analysis-basics.
3. Keysight, Real-time Spectrum Analyzers N9040B. https://literature.cdn.keysight.com/litweb/pdf/5991-1748EN.pdf?id=2303225.
4. C. Laperle and M. O'Sullivan, "Advances in high-speed DACs, ADCs, and DSP for optical coherent transceivers," J. Lightwave Technol. **32**(4), 629–643 (2014).
5. P. Berger, Y. Attal, M. Schwarz, S. Molin, A. Louchet-Chauvet, T. Chanelière, J.-L. Le Gouët, D. Dolfi, and L. Morvan, "RF spectrum analyzer for pulsed signals: ultra-wide instantaneous bandwidth, high sensitivity, and high time-resolution," J. Lightwave Technol. **34**(20), 4658–4663 (2016).
6. K. Merkel, S. Bekker, A. Traxinger, C. Stiffler, A. Woidtke, M. Chase, R. Babbitt, C. Harrington, and Z. Barber, "Extreme bandwidth spectrum analysis," *Proceeding of 2016 IEEE Photonics Conference (IPC) Waikoloa*, HI, USA, p. 487–488 (2017).
7. X. Zou, B. Lu, W. Pan, A. Stöhr, and J. Yao, "Photonics for microwave measurements," Laser Photonics Rev. **10**(5), 711–734 (2016).
8. L. Romero Cortés, D. Onori, H. Guillet de Chatellus, M. Burla, and J. Aza na, "Towards on-chip photonic-assisted radio-frequency spectral measurement and monitoring," Optica **7**(5), 434–447 (2020).
9. R. Salem, M. A. Foster, and A. L. Gaeta, "Application of space–time duality to ultrahigh-speed optical signal processing," Adv. Opt. Photonics **5**(3), 274–317 (2013).
10. T. Jannson, "Real-time Fourier transformation in dispersive optical fibers," Opt. Lett. **8**(4), 232–234 (1983).
11. K. Goda and B. Jalali, "Dispersive Fourier transformation for fast continuous single-shot measurements," Nat. Photonics **7**(2), 102–112 (2013).

OPTICS CONTINUUM

12. R. E. Saperstein, D. Panasenko, and Y. Fainman, "Demonstration of a microwave spectrum analyzer based on time-domain optical processing in fiber," Opt. Lett. **29**(5), 501–503 (2004).
13. S. R. Konatham, R. Maram, L. Romero Cortés, J. H. Chang, L. Rusch, S. LaRochelle, H. Guillet de Chatellus, and J. Aza na, "Real-time gap-free dynamic waveform spectral analysis with nanosecond resolutions through analog signal processing," Nat. Commun. **11**(1), 3309 (2020).
14. H. Guillet de Chatellus, L. Romero Cortés, and J. Azana, "Optical real-time Fourier transformation with kilohertz resolutions," Optica **3**(1), 1–8 (2016).
15. Patent FR2012783, "Dispositif d'analyse spectrale large bande d'un signal d'intérêt," CNRS/Université Grenoble Alpes.
16. H. Guillet de Chatellus, E. Lacot, W. Glastre, O. Jacquin, and O. Hugon, "Theory of Talbot lasers," Phys. Rev. A **88**(3), 033828 (2013).
17. H. Guillet de Chatellus, O. Jacquin, O. Hugon, W. Glastre, E. Lacot, and J. Marklof, "Generation of ultrahigh and tunable repetition rates in CW injection-seeded frequency-shifted feedback lasers," Opt. Express **21**(13), 15065–15074 (2013).
18. C. Schnébelin and H. Guillet de Chatellus, "Agile photonic fractional Fourier transformation of optical and RF signals," Optica **4**(8), 907 (2017).
19. V. Duran, L. Djevarhidjian, and H. Guillet de Chatellus, "Bidirectional frequency-shifting loop for dual-comb spectroscopy," Opt. Lett. **44**(15), 3789–3792 (2019).
20. V. Billault, V. Duran, C. R. Fernández-Pousa, V. Crozatier, D. Dolfi, and H. Guillet de Chatellus, "All-optical coherent pulse compression for dynamic laser ranging using an acousto-optic dual comb," Opt. Express **29**(14), 21369–21385 (2021).
21. G. Bourdarot, J.-P. Berger, and H. Guillet de Chatellus, "Multi-delay photonic correlator for wideband RF signal processing," Optica **9**(4), 325–334 (2022).
22. N. Kanagaraj, L. Djevarhidjian, V. Duran, C. Schnébelin, and H. Guillet de Chatellus, "Optimization of acousto-optic optical frequency combs," Opt. Express **27**(10), 14842–14852 (2019).
23. I. Coddington, N. Newbury, and W. Swann, "Dual-comb spectroscopy," Optica **3**(4), 414–426 (2016).
24. C. Fernández-Pousa and H. Guillet de Chatellus, "Fundamental SNR limits imposed by ASE in frequency-shifting loops," J. Lightwave Technol. **40**(20), 6831–6844 (2022).